J|A|C|S ARTICLES

Published on Web 04/28/2010

Metal Inorganic Frameworks: Dynamic Flexible Architecture with Extended Pore Order Built from $[Se_3]^{2-}$ Linkers and $[Re_6Se_6Br_8]^{2-}$ Clusters

Nan Ding,[†,‡] Gerasimos S. Armatas,[†,§] and Mercouri G. Kanatzidis*[,†,||]

Department of Chemistry, Northwestern University, Evanston, Illinois 60208, Department of Chemistry, Claflin University, Orangeburg, South Carolina 29115, Department of Materials Science and Technology, University of Crete, 71003 Heraklion, Greece, and Materials Science Division, Argonne National Laboratory, Argonne, Illinois 60439

Received December 13, 2009; E-mail: m-kanatzidis@northwestern.edu

Abstract: A mesostructured chalcogenide built from Chevrel-type clusters $[(Re_6Se_6Br_2)Br_6^T]^{2-}$ linked by ditopic $[Se_3]^{2-}$ anions and synthesized in the presence of a cationic surfactant template is reported. This new mesophase, *h*-C_{18}PyReSeBr, exhibits remarkably well ordered hexagonal symmetry from which a reasonable structural model can be deduced on the basis of powder X-ray diffraction as well as pair distribution function (PDF) analysis. Small-angle X-ray scattering (SAXS) analysis shows that *h*-C_{18}PyReSeBr possesses an enormous interfacial area of 477 m^2/g between the inorganic framework and the guest surfactant cations, which is comparable to that of mesoporous silicas when heavy metals contained in the framework are taken into consideration. The framework of *h*-C_{18}PyReSeBr exhibits great flexibility and responds dynamically to the extraframework cations via an ion-exchange process.

Introduction

Mesostructured silicates such as MCM-41 and SBA-15 or transition-metal oxide frameworks are produced via the structure-directing assistance of soft or hard templates.[1−4] These materials possess a well-defined mesoscopic pore order but have inorganic frameworks that are random and lack atomic periodicity. Recently, a few MCM-41-type organosilicas,[5] a couple of covalent organic frameworks COF-5[6a] and COF-108,[6b] and a crystalline cubic germanium oxide[7] were reported to have not only periodic mesopores but also frameworks with well-defined molecular structure.

A recent development in mesoporous materials is the emergence of mesostructured chalcogenides that feature electronically "active" frameworks.[8−10] These chalcogenides are typically assembled via coordination reactions between a building-block anion (e.g., $Ge_4S_{10}^{4-}$) and a linking metal cation.[8] The availability of many building blocks makes it possible to produce a diverse set of surfactant-templated metal chalcogenides with well-ordered mesostructures and useful functionalities.[9,10] However, because of the lack of atomic periodicity a molecular structure model for these compounds has yet to be provided. In this work, we used Chevrel-type clusters $[(Re_6Se_6Br_2)Br_6^T]^{2-}$ (where Br^T represents the terminal Br atoms

[†] Northwestern University.
[‡] Claflin University.
[§] University of Crete.
[||] Argonne National Laboratory.

(1) (a) Beck, J. S.; Vartuli, J. C.; Roth, W. J.; Leonowicz, M. E.; Kresge, C. T.; Schmitt, K. D.; Chu, C. T. W.; Olson, D. H.; Sheppard, E. W. *J. Am. Chem. Soc.* **1992**, *114*, 10834. (b) Huo, Q.; Margolese, D. I.; Ciesla, U.; Feng, P.; Gier, T. E.; Sieger, P.; Leon, R.; Petroff, P. M.; Schüth, F.; Stucky, G. D. *Nature* **1994**, *368*, 317. (c) Sayari, A.; Hamoudi, S. *Chem. Mater.* **2001**, *13*, 3151.
(2) (a) Zhao, D.; Feng, J.; Huo, Q.; Melosh, N.; Fredrickson, G. H.; Chmelka, B. F.; Stucky, G. D. *Science* **1998**, *279*, 548. (b) Zhao, D.; Huo, Q.; Feng, J.; Chmelka, B. F.; Stucky, G. D. *J. Am. Chem. Soc.* **1998**, *120*, 6024. (c) Kim, M. J.; Ryoo, R. *Chem. Mater.* **1999**, *11*, 487.
(3) (a) Ciesla, U.; Demuth, D.; Leon, R.; Petroff, P.; Stucky, G. D.; Unger, K.; Schuth, F. *Chem. Commun.* **1994**, *11*, 1387. (b) Wang, Y.; Ma, C.; Sun, X.; Li, H. J. *J. Colloid Interface Sci.* **2005**, *286*, 627. (c) Antonelli, D.; Ying, J. Y. *Angew. Chem., Int. Ed.* **1995**, *34*, 2014.
(4) (a) Yang, P.; Zhao, D.; Margolese, D. I.; Chmelka, B. F.; Stucky, G. D. *Nature* **1998**, *396*, 152. (b) Liu, Y.; Zhang, W.; Pinnavaia, T. J. *Angew. Chem., Int. Ed.* **2001**, *40*, 1255.
(5) (a) Inagaki, S.; Guan, S.; Ohsuna, T.; Terasaki, O. *Nature* **2002**, *416*, 304. (b) Sayari, A.; Wang, W. *J. Am. Chem. Soc.* **2005**, *127*, 12194.
(6) (a) Côté, A. P.; Benin, A. I.; Ockwig, N. W.; O'Keeffe, M.; Matzger, A.; Yaghi, O. M. *Science* **2005**, *310*, 1166. (b) El-Kaderi, H. M.; Hunt, J. R.; Mendoza-Cortés, J. L.; Côté, A. P.; Taylor, R. E.; O'Keeffe, M.; Yaghi, O. M. *Science* **2007**, *316*, 268.
(7) Zou, X.; Conradsson, T.; Klingstedt, M.; Dadachov, M. S.; O'Keeffe, M. *Nature* **2005**, *437*, 716.
(8) (a) MacLachlan, M. J.; Coombs, N.; Ozin, G. A. *Nature* **1999**, *397*, 681. (b) MacLachlan, M. J.; Coombs, N.; Bedard, R. L.; White, S.; Thompson, L. K.; Ozin, G. A. *J. Am. Chem. Soc.* **1999**, *121*, 12005.
(9) (a) Riley, A. E.; Tolbert, S. H. *J. Am. Chem. Soc.* **2003**, *125*, 4551. (b) Korlann, S. D.; Riley, A. E.; Kirsch, B. L.; Mun, S.; Tolbert, S. H. *J. Am. Chem. Soc.* **2005**, *127*, 12516.
(10) (a) Trikalitis, P. N.; Rangan, K. K.; Bakas, T.; Kanatzidis, M. G. *Nature* **2001**, *410*, 671. (b) Wachhold, M.; Rangan, K. K.; Lei, M.; Thorpe, M. F.; Billinge, S. J. L.; Petkov, V.; Heising, J.; Kanatzidis, M. G. *J. Solid State Chem.* **2000**, *152*, 21. (c) Wachhold, M.; Rangan, K. K.; Billinge, S. J. L.; Petkov, V.; Heising, J.; Kanatzidis, M. G. *Adv. Mater.* **2000**, *12*, 85. (d) Rangan, K. K.; Trikalitis, P. N.; Bakas, T.; Kanatzidis, M. G. *Chem. Commun.* **2001**, 809. (e) Rangan, K. K.; Billinge, S. J. L.; Petkov, V.; Heising, J.; Kanatzidis, M. G. *Chem. Mater.* **1999**, *11*, 2629. (f) Rangan, K. K.; Trikalitis, P. N.; Canlas, C.; Bakas, T.; Weliky, D. P.; Kanatzidis, M. G. *Nano Lett.* **2002**, *2*, 513. (g) Trikalitis, P. N.; Rangan, K. K.; Bakas, T.; Kanatzidis, M. G. *J. Am. Chem. Soc.* **2002**, *124*, 12255. (h) Kanatzidis, M. G. *Adv. Mater.* **2007**, *19*, 1165. (i) Armatas, G. S.; Kanatzidis, M. G. *Nat. Mater.* **2009**, *8*, 217.

 10.1021/ja910506b

of the cluster)[11] as the building block and obtained a new hexagonal mesophase *h*-C_{18}PyReSeBr (where C_{18}Py represents the alkyl-pyridinium surfactant cations present in the material). The framework is remarkably well ordered, which allowed us to deduce a reasonable molecular structure model for this chalcogen-based mesostructure. The redox-active and ligand-substitution properties of the hexarhenium chalcogenide clusters $[Re_6Q_8]^{2+}$ (Q = S, Se, and Te) represent attractive building blocks for the construction of well-defined functional mesostructures.[12−14] Only a few examples of mesoporous materials built from redox clusters are known,[15] yet they promise to add new capability, including redox-based catalytic function and reversible storage of reducing equivalents. Recently, the metal-mediated assembly of $[Re_6Q_8(CN)_6)]^{4-}$ (Q = S, Se, and Te) clusters to form hexagonal and lamellar cyanide-based mesostructures has been described.[16]

The linkers within *h*-C_{18}PyReSeBr are the ditopic polyselenide anions $[Se_3]^{2-}$. To our knowledge, this is the first example of polyselenide anions $[Se_x]^{2-}$ being used for the construction of surfactant-templated assemblies. In contrast to the structurally rigid hexarhenium clusters, the $[Se_3]^{2-}$ anion, with its flexible bond angles, acts as a "joint" between two $[(Re_6Se_6Br_2)Br_6^T]^{2-}$ clusters. Indeed, ion exchange of the surfactant cations in *h*-C_{18}PyReSeBr by H^+ is accompanied by the dynamic reversible response of the framework, resulting in large volume changes.[17] Such framework flexibility is relevant to potential sensor and actuator applications;[18] however, most of the studies on this topic are focused on coordination polymers[18,19] and organic/inorganic hybrids.[20] *h*-C_{18}PyReSeBr is one of the few compounds whose framework flexibility is derived from the ability of the ditopic linkers to twist and bend around Se−Se bonds.

Experimental Section

Syntheses. Starting Materials. K_2Se_3 was synthesized by the direct combination of K_2Se and Se in a 13 mm quartz tube that was flame sealed under vacuum and held at ∼900 °C for 3 days. Octadecylpyridinium bromide was synthesized by reacting the corresponding 1-bromooctadecane with excess pyridine in ethanol under reflux conditions. Recrystallization from $CHCl_3$−ethyl acetate was used to purify the compounds. $[(C_6H_5)_4P]_2[Re_6Se_6Br_8]$ was synthesized according to ref 11.

Synthesis of *h*-C_{18}PyReSeBr. Inside a nitrogen-filled glovebox, 2.0 g of C_{18}PyBr surfactant was dissolved in 10 mL of formamide. The mixture was stirred at 80 °C for about 10−15 min. Meanwhile, 0.078 g of K_2Se_3 was dissolved in 3 mL of formamide, forming a dark-red solution, and 0.18 g of $[(C_6H_5)_4P]_2[Re_6Se_6Br_8]$ was dissolved in 3 mL of *N*,*N*′-dimethylformamide (DMF), forming clear red solution. These two solutions were then simultaneously added dropwise to the surfactant/FM solution over a period of 20 min. A dark-brown precipitate formed after a few drops of the starting materials were added to the surfactant solution. The product was stirred at 80 °C overnight, filtered off, washed with copious amounts of warm formamide, DMF, and water, and then dried under vacuum. The filtrate was yellow-orange, and the yield was >90% on the basis of the cluster.

H^+-Exchange Experiment. *h*-C_{18}PyReSeBr (∼0.2 g) was added to a mixed solution of 10 mL of conc HCl and 40 mL of ethanol. The mixture was stirred under reflux conditions for ∼5 h. The product was filtered off and washed with copious amounts of warm formamide and water and then dried under vacuum. The filtrate was colorless.

Inductively Coupled Plasma-Atomic Emission (Optical Emission) [ICP-AES(OES)] Analyses. The Re, Br, and Se contents of the *h*-C_{18}PyReSeBr materials were also determined by ICP-AES using a Vista MPX CCD simultaneous ICP-OES instrument. Re, Br, and Se standards were prepared in the range 0.1−1 ppm by diluted commercial (Aldrich or GFS Chemicals) 1000 ppm ICP standard. The calibration was linear with an error of <5%. The ICP-AES intensity was the result of three (30 s) exposures. For each sample, three readings of the ICP-AES intensity were recorded and averaged.

X-ray Data Collection, Unit Cell Determination, and Le Bail Extraction. Powder X-ray diffraction (XRD) was performed on a Rigaku Rotaflex diffractometer equipped with Ni-filtered Cu Kα radiation (λ = 1.5405 Å) at 45 kV and 100 mA in Bragg−Brentano geometry. A silver behenate standard was used for low-angle calibration of the instrument.[21] The sample was gently ground and placed on a zero-background glass holder, and the surface was smoothed carefully using a glass slice. For the construction of a structural model, XRD data were recorded in the range of $2\theta = 1.5-20°$ using a scan rate of 0.01° and an exposure time of 10 s in step mode.

Peak searching was performed using WinPLOTR (Jan 2006 version) software,[22] and the crystal symmetry and lattice parameters were determined using automatic powder pattern indexing program Dicvol91.[23] When the first seven strongest reflections were used, a hexagonal unit cell was found with a = 44.89 (0.08) Å and c = 10.74 (0.03) Å (V = 18742.38 Å^3) (figures of merit: M_7 = 41.7 and F_7 = 58.7).

Subsequently, the entire powder pattern decomposition was performed using FullProf (July 2001 version) software,[24] and the LeBail algorithm was applied.[25] Background intensities were first

(11) In $(Ph_4P)_2[Re_6Se_6Br_2]Br_6$, six Se atoms and two Br atoms have mixed occupancy at the μ_3 bridging sites around the Re_6 octahedron. The other six Br atoms are terminal and can be replaced by other ligands (in this case, the $[Se_3]^{2-}$ ions). See Yarovoi, S. S.; Solodovnikov, S. F.; Tkachev, S. V.; Mironov, Yu. V.; Fedorov, V. E. *Russ. Chem. Bull., Int. Ed.* **2003**, *5*, 68.

(12) (a) Gray, T. G.; Rudzinski, C. M.; Meyer, E. E.; Holm, R. H.; Nocera, D. G. *J. Am. Chem. Soc.* **2003**, *125*, 4755. (b) Chen, Z.-N.; Yoshimura, T.; Abe, M.; Tsuge, K.; Sasaki, Y.; Ishizaka, S.; Kim, H.-B.; Kitamura, N. *Chem.−Eur. J.* **2001**, *7*, 4447.

(13) (a) Willer, M. W.; Long, J. R.; McLauchlan, C. C.; Holm, R. H. *Inorg. Chem.* **1998**, *37*, 328–333. (b) Zheng, Z. P.; Long, J. R.; Holm, R. H. *J. Am. Chem. Soc.* **1997**, *119*, 2163–2171.

(14) (a) Roland, B. K.; Flora, W. H.; Selby, H. D.; Armstrong, N. R.; Zheng, Z. P. *J. Am. Chem. Soc.* **2006**, *128*, 6620–6625. (b) Roland, B. K.; Selby, H. D.; Carducci, M. D.; Zheng, Z. P. *J. Am. Chem. Soc.* **2002**, *124*, 3222–3223. (c) Selby, H. D.; Roland, B. K.; Zheng, Z. P. *Acc. Chem. Res.* **2003**, *36*, 933–944. (d) Zheng, Z. P.; Tu, X. Y. *CrystEngComm* **2009**, *11*, 707–719.

(15) Trikalitis, P. N.; Bakas, T.; Papaefthymiou, V.; Kanatzidis, M. G. *Angew. Chem., Int. Ed.* **2000**, *39*, 4558.

(16) (a) Suh, M.-J.; Vien, V.; Huh, S.; Kim, Y.; Kim, S.-J. *Eur. J. Inorg. Chem.* **2008**, 686. (b) Vien, V.; Suh, M.-J.; Huh, S.; Kim, Y.; Kim, S.-J. *Chem Commun.* **2009**, 541.

(17) Trikalitis, P. N.; Ding, N.; Malliakas, C.; Billinge, S. J. L.; Kanatzidis, M. G. *J. Am. Chem. Soc.* **2004**, *126*, 15326.

(18) (a) Zhang, J.-P.; Chen, X.-M. *J. Am. Chem. Soc.* **2008**, *130*, 6010. (b) Huang, S. P.; Kanatzidis, M. G. *Inorg. Chem.* **1991**, *30*, 1455–1466. (c) Kanatzidis, M. G.; Huang, S. P. *Inorg. Chem.* **1989**, *28*, 4667–4669. (d) Kanatzidis, M. G.; Huang, S. P. *J. Am. Chem. Soc.* **1989**, *111*, 760–761. (e) Kim, K. W.; Kanatzidis, M. G. *Inorg. Chem.* **1993**, *32*, 4161–4163. (f) Kim, K. W.; Kanatzidis, M. G. *J. Am. Chem. Soc.* **1998**, *120*, 8124–8135.

(19) Kitagawa, S.; Uemura, K. *Chem. Soc. Rev.* **2005**, *34*, 109.

(20) Férey, G. *Chem. Soc. Rev.* **2008**, *37*, 191.

(21) Huang, T. C.; Toraya, H.; Blanton, T. N.; Wu, Y. *J. Appl. Crystallogr.* **1993**, *26*, 180.

(22) Roisnel, T. J.; Rodríguez-Carvajal, J. *Materials Science Forum, Proceedings of the Seventh European Powder Diffraction Conference (EPDIC 7)*; Delhez, R., Mittenmeijer, E. J., Eds.; 2000, pp 118−123.

(23) Boultif, A.; Louer, D. *J. Appl. Crystallogr.* **2004**, *37*, 724.

(24) Rodriguez-Carvajal, J. *Abstracts of the Satellite Meeting on Powder Diffraction of the XV Congress of the IUCr*; Toulouse, France, 1990, p 127.

(25) LeBail, A.; Duroy, H.; Fourquet, J. L. *Mater. Res. Bull.* **1988**, *23*, 447.

hand-fit and next refined together with the pseudo-Voigt peak-shape profile, zero shift, and polarization parameters. We determined the unit cell parameters by indexing the powder pattern and the peak asymmetry using a Finger−Cox−Jephcoat correction.[26] Refinement of the cell parameters and peak asymmetry led to optimum agreement between the simulated (Figure S1) and experimental powder diffraction patterns. A hexagonal unit cell with parameters of $a = 44.497$ (7) Å and $c = 11.123$ (1) Å ($V = 19072.0$ Å^3) was obtained after convergent refinement ($R_p = 2.68$, $R_{wp} = 3.38$, and $R_{exp} = 7.08$).

Pair Distribution Function (PDF) Analysis. A diffraction experiment was carried out using X-ray high-energy synchrotron radiation (90.48 KeV, $\lambda = 0.13702$ Å) at Argonne National Laboratory. The collected images were 2D, and they were reduced to 1D plots of $I(q) = f(q)$, where q is the wavevector using the FIT2D program.[27] Diffraction data were corrected for the polarization beam and empty-cell scattering.

Small-Angle X-ray Scattering (SAXS) Analysis. The SAXS patterns were collected on a Rigaku S-MAX 3000 high-brilliance system equipped with a 2D wire detector and a Cu ($\lambda = 1.54098$ Å) rotating anode operated at 80 kV and 40 mA ($0.01 < q < 0.6$ Å^{-1}). Measurements were performed by transmission on samples that were gently ground and held in a custom-built cell. The sample cell had Kapton windows (~4 mm width) and was ~40 μm thick. The sample-to-detector distance and the center of the beam were precisely determined by calibration with a Ag-behenate diffraction standard ($d_{001} = 58.38$ Å). The diffraction intensities of the 2D collected images were integrated to yield 1D diffraction patterns as a function of q with the FIT2D program.[28] Scattering data were corrected for the dark current and empty cell scattering.

The internal surface area (S_p) of the structural model of h-C_{18}PyReSeBr was determined according the following equation

$$S_p(\mathrm{m}^2/\mathrm{g}) = \frac{2\pi c\left(\frac{D_p}{2}\right)}{\mathrm{vol}\ d_b} \times 10^4$$

where c is the length of the unit cell parallel to the pore channel axis (= 11.1227 Å), D_p is the pore size (= 35 Å), vol is the volume of the unit cell (= 19 072.01 Å^3), and d_b is the bulk density (= 1.3 g/cm^3) of the inorganic model. The bulk density of the inorganic structure of h-C_{18}PyReSeBr was calculated from the structural model according to the equation

$$d_b = Z(\mathrm{MW}_{\mathrm{inorg}})/N_a/\mathrm{vol}$$

where $Z = 6$, $\mathrm{MW}_{\mathrm{inorg}}$ is the molecular weight of the inorganic phase in g/mol, N_a is Avogadro's number in mol^{-1}, and vol is the volume of the unit cell in cm^3.

Physical Measurements. Powder XRD patterns were acquired on a calibrated Rigaku Rotaflex diffractometer (45 kV, 100 mA) using a rotating anode Cu Kα radiation source. In the 2θ range of 1−60°, the scan rate was 0.10°/min with a step size of 0.02°.

Quantitative microprobe analyses were performed on a JEOL JSM-6400 V scanning electron microscope (SEM) equipped with a Noran energy dispersive spectroscopy (EDS) detector. Data acquisition was performed with an accelerating voltage of 20 kV and a 60 s accumulation time.

High-resolution transmission electron micrographs (TEM) were obtained with a JEOL 120CX instrument equipped with a CeB_6 filament operating at 120 kV. The samples were gently ground and suspended in ethyl ether in a glovebox. A holey carbon grid was dipped into the suspension and dried in air prior to the TEM experiments.

Elemental C, H, and N analyses were obtained on a Perkin-Elmer Series II CHNS/O Analyzer 2400.

Thermogravimetric analysis (TGA) was performed using a computer-controlled Shimadzu TGA-50 thermal analyzer. Typically, 20 mg of sample was placed in a silica bucket and heated under a nitrogen flow of 20 mL/min at a rate of 10 °C/min.

Raman spectra (3500−100 cm^{-1}) were recorded on a computer-controlled Bio-Rad Fourier transform (FT) Raman spectrometer with a Spectra-Physics Topaz T10-106c 1064 nm YAG laser. The instrument was configured in 180° backscattering mode, and the samples were loaded into melting-point capillary tubes.

UV/vis/near-IR diffuse reflectance spectra were obtained at room temperature on a Shimadzu UV-3101PC double-beam, double-monochromator spectrophotometer in the wavelength range of 200−2500 nm. $BaSO_4$ powder was used as a reference (100% reflectance) and the base material onto which the powder sample was coated. Reflectance data were converted to absorbance data as described elsewhere.[29]

Results and Discussion

The synthesis of hexagonal h-C_{18}PyReSeBr with a crystal-like pore framework was achieved via the metathesis reaction between $(Ph_4P)_2[(Re_6Se_6Br_2)Br_6^T]$ and K_2Se_3 (1:4 molar ratio) along with excess surfactant in which the $[Se_3]^{2-}$ anions are believed to connect the octahedral $[(Re_6Se_6Br_2)Br_6^T]^{2-}$ clusters by replacing the six terminal Br^T ions, as illustrated in Scheme 1.

The XRD pattern of the product exhibits up to 17 Bragg diffraction peaks in the range of $2° < 2\theta < 17°$ (Figure 1). This is more than any other surfactant-templated mesoporous solid. For example, in well-ordered mesostructured silicas[1a,30] or metal chalcogenides[8−10] only four or five reflections are typically observed. The direct examination of a h-C_{18}PyReSeBr sample with transmission electron microscopy (TEM) clearly shows hexagonally ordered pore channels (Figure 2). The fast Fourier transform (FFT) pattern confirms the extended mesoscopic pore ordering by clearly showing high-index reflections. The mesoscale order of this material is robust and has a high driving force because varying the reaction temperature by ±20 °C or reducing the amount of surfactant by half does not change the hexagonal arrangement of the pores. The high-angle ($2\theta > 6°$) Bragg reflections, which indicate long-range order, are consistent with the $P6/mmm$ space group. The lattice parameters refined from the diffraction pattern were $a = 44.497(7)$ Å and $c = 11.123(1)$ Å. Details are described in Supporting Information, and the observed reflections, along with indexing, are listed in Table S1.

The Raman spectra (Figure 3) of h-C_{18}PyReSeBr and proton-exchanged h-H^+/C_{18}PyReSeBr materials show shifts in the 150−300 cm^{-1} region that are similar to the spectra of $(Ph_4P)_2Re_6Se_6Br_8$ and K_2Se_3 compounds, consistent with the presence of $[(Re_6Se_6Br_2)Br_6^T]^{2-}$ units linked with Se_3^{2-} ligands.[31] In the spectrum of the free cluster, the Raman shift centered at 284 cm^{-1} is attributed to a breathing vibration of the Re_6 core, which in h-C_{18}PyReSeBr moves to a slightly higher wavenumber at 297 cm^{-1}. The Raman peak centered at 188 cm^{-1} in the spectrum of the free cluster is possibly due to the

(26) Finger, L. W.; Cox, D. E.; Jephcoat, A. P. *J. Appl. Crystallogr.* **1994**, *27*, 892.
(27) Billinge, S. J.; Kanatzidis, L, M. G. *Chem. Commun.* **2004**, 749.
(28) Hammersley, F. A. P. *ESRF98HA01T: FIT2D V9.129 Reference Manual V3.1*, Internal Report.; ESRF: France, 1998.
(29) (a) Kortüm, G. *Reflectance Spectroscopy: Principles, Methods, Applications*: Springer, Berlin, 1969. (b) Liao, J. H.; Varotsis, C.; Kanatzidis, M. G. *Inorg. Chem.* **1993**, *32*, 2453–2462.
(30) (a) Kruk, M.; Jaroniec, M. *Chem. Mater.* **1999**, *11*, 1568. (b) Huo, Q.; Margolese, D.; Stucky, G. D. *Chem. Mater.* **1996**, *8*, 1147. (c) Sakamoto, Y.; Kaneda, M.; Terasaki, O.; Zhao, D.; Kim, J.-M.; Stucky, G. D.; Shin, H. J.; Ryoo, R. *Nature* **2000**, *408*, 449.
(31) The assignment of the Raman shifts is based on Selby, H. D.; Roland, B. K.; Zheng, Z. *Acc. Chem. Res.* **2003**, *36*, 933.

Scheme 1. Illustration of the Metathesis Reaction between the Octahedral $[(Re_6Se_6Br_2)Br_6^T]^{2-}$ Cluster with Triselenide Anions[a]

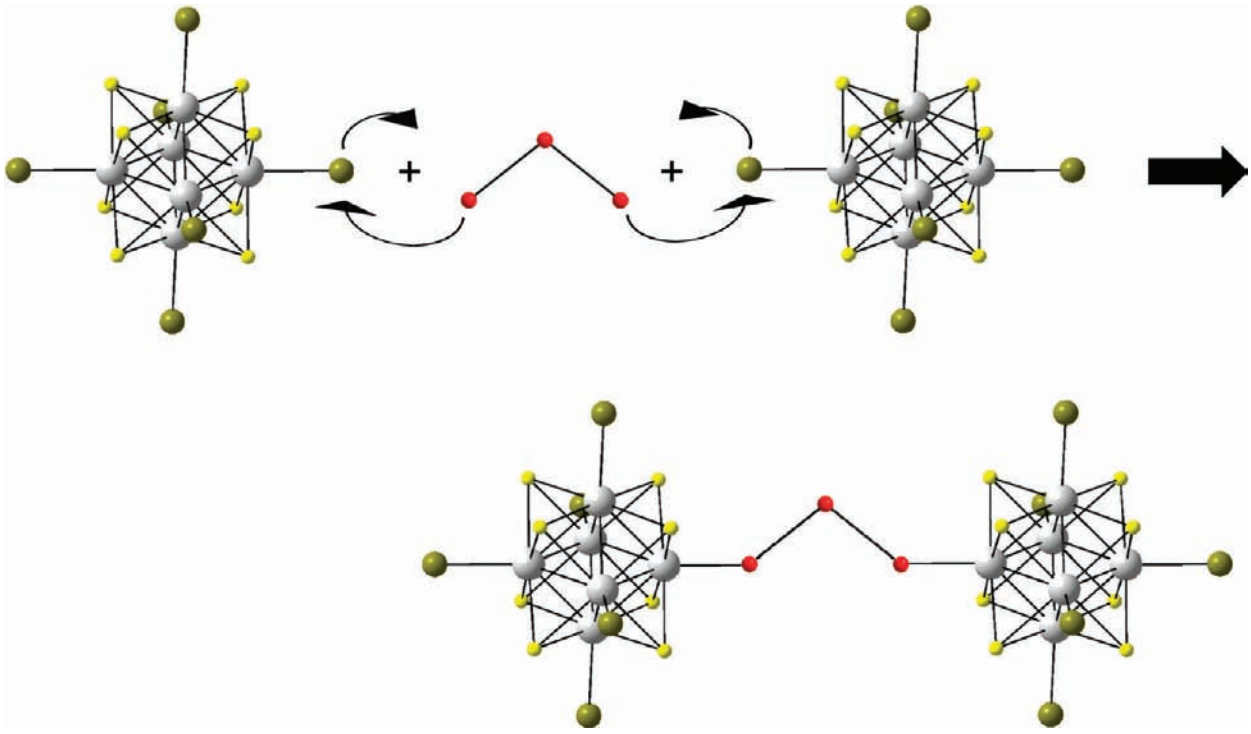

[a] Grey atoms are Re, yellow atoms are mixed occupied Se/Br (designated as E in the text), red atoms are Se, and brown atoms are Br.

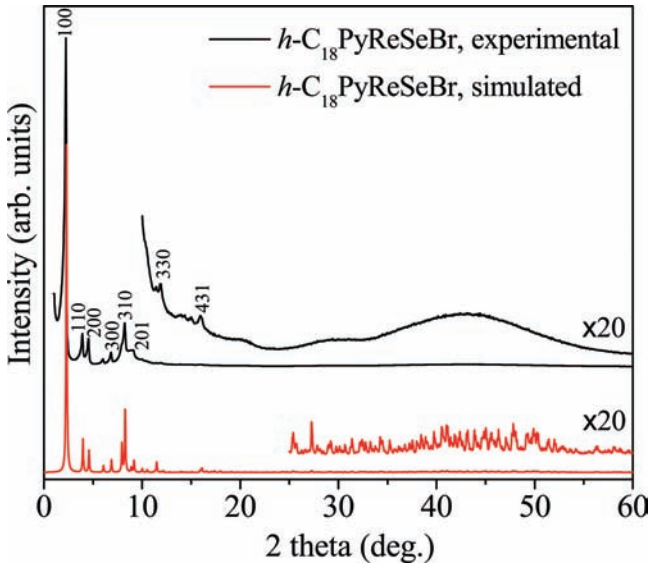

Figure 1. Powder XRD patterns of *h*-C_{18}PyReSeBr: experimental (black) and simulated from the structural model of *h*-C_{18}PyReSeBr (red).

totally symmetric vibration of the Br_6^T atoms, which is not observed in the spectrum of *h*-C_{18}PyReSeBr because the terminal atoms are now Se (from the $[Se_3]^{2-}$ linking units). The bands at 164 cm^{-1} and those in the range of 219−251 cm^{-1} in the spectrum of $(Ph_4P)_2[(Re_6Se_6Br_2)Br_6^T]$ are tentatively assigned as E_g and T_{2g} vibrational modes of the O_h-symmetric cluster. The breathing vibration of the eight tricapping (Se_6Br_2) atoms may be also covered within this range. These bands are rather obscure in the mesostructrued phases, probably because of broadening due to distribution lowering in the symmetry of the ($Re_6Se_6Br_2$) core.

To probe the existence of the cluster core $(Re_6Se_6Br_2)^{4+}$ in the metal inorganic framework further, we conducted diffuse scattering measurements and pair distribution function (PDF) analysis.[27] Figure 4 shows the experimental PDF plots of *h*-C_{18}PyReSeBr and the starting material $(Ph_4P)_2[(Re_6Se_6Br_2)Br_6^T]$ as well as the theoretical PDF plot from the structural model of *h*-C_{18}PyReSeBr (see below.) It is apparent that the PDF plots of the *h*-C_{18}PyReSeBr material and $(Ph_4P)_2[(Re_6Se_6Br_2)Br_6^T]$ are very similar in the region of $r < 7$ Å, indicating similar local atomic structure. The pair correlation peak at 2.6 Å corresponds to Re−Re bond distances in the cluster;[32] those at ∼3.7 Å arise from the nonbonding diagonal Re···Re distances, and the peaks at ∼4.6 Å are caused by the next-nearest-neighbor distances of Re···Se and Re···Br^T in the octahedral $[(Re_6Se_6Br_2)Br_6^T]$ unit. The theoretical PDF derived from the structural model of *h*-C_{18}PyReSeBr (discussed below) is also in good agreement with the experimental one.

On the basis of the available data (i.e., unit cell parameter elemental analysis, PDF results, spectroscopy, and X-ray diffraction patterns), several structure models were explored. The one shown in Figure 5 is consistent with the experimental data. The corresponding powder XRD patterns from the various models were generated using ICSD Visualizer (version 1.0.1.2)[33] to compare with the experimental data. While maintaining chemical rationality, the structural details of the model were adjusted until the simulated XRD pattern exhibited an excellent match with the experimental one, as shown in Figure 1.

Figure 5 shows the structural model of the *h*-C_{18}PyReSeBr material. As illustrated in Scheme 1, all six terminal Br^T atoms of each $[(Re_6Se_6Br_2)Br_6^T]^{2-}$ cluster are replaced by triselenide

(32) The direct Re−Se bonds are ∼2.48 Å long, and the Se−Se bonds are ∼ 2.38 Å long; both fall in the region of the peak centered at 2.6 Å. Therefore, this pair correlation peak also has contributions from the Re−Se and Se−Se bonds.

(33) Bergerhoff, G.; Brown, I. D. In *Crystallographic Databases*, Allen, F. H. et al. Eds.; International Union of Crystallography, Chester, England, 1987.

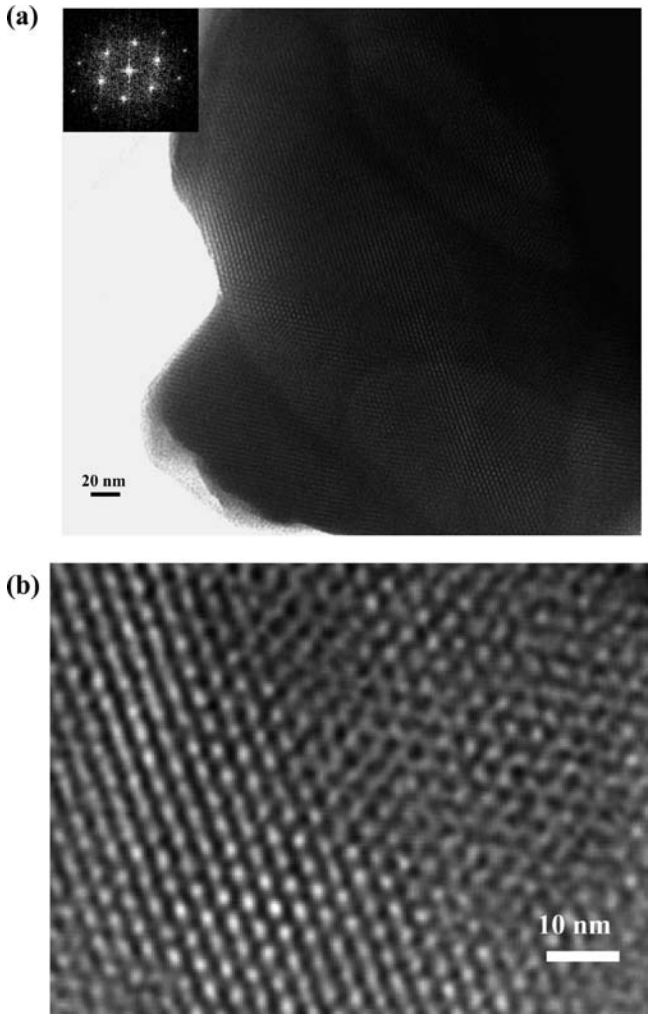

Figure 2. (a) Representative TEM image of *h*-C_{18}PyReSeBr, with the view parallel to the hexagonal pores. The insets show the corresponding FFT pattern that is consistent with the highly ordered hexagonal symmetry. (b) Higher-magnification region showing the extended hexagonal arrangement of the structure.

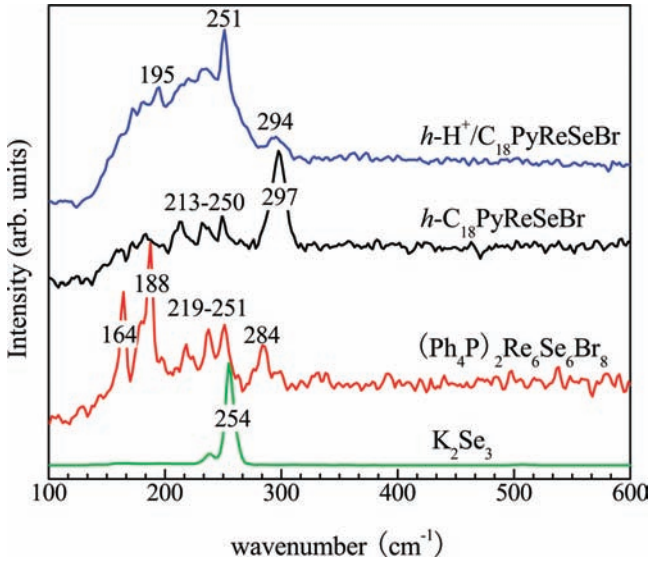

Figure 3. Raman spectra of *h*-C_{18}PyReSeBr, *h*-H^+/C_{18}PyReSeBr, $(Ph_4P)_2$-$[(Re_6Se_6Br_2)Br_6^T]$, and K_2Se_3 materials.

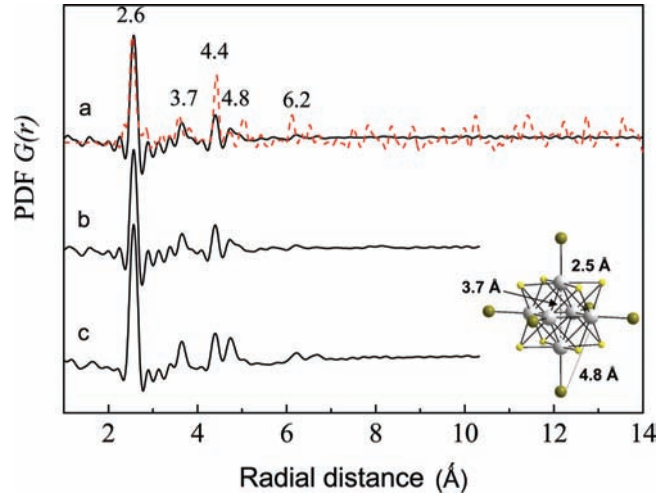

Figure 4. Reduced atomic pair distribution function $G(r)$ for (a) *h*-C_{18}PyReSeBr (dotted line representing the corresponding PDF plot calculated from the structural model of *h*-C_{18}PyReSeBr), (b) *h*-H^+/C_{18}PyReSeBr, and (c) $(Ph_4P)_2[(Re_6Se_6Br_2)Br_6^T]$ materials.

ligands to form a 3D architecture. The smallest distance within one hexagonal pore is ~35 Å, and the wall thickness is about 9.5 Å (including the van der Waals radii). Because the core of the $[(Re_6Se_6Br_2)Br_6^T]^{2-}$ cluster is intact, we assumed the bond distances and angles of this unit to be invariant from those of the starting material (i.e., Re−Re ≈ 2.61 Å; Re−E ≈ 2.53 Å, where E represents the Se and Br atoms in the cluster core). The $[Se_3]^{2-}$ fragment, however, acts as a strut and can be more flexible, especially around the Se−Se−Se or Re−Se−Se bonds and dihedral angles. The experimental unit cell dimensions and regular bond lengths were fixed and the angles were varied to arrive at the structural model (Tables S2 and S3). It is important to point out that further structural details are beyond the limit of what can be obtained from the XRD data, and relative twist/rotation/bending modes among the building blocks are most likely present but are not taken into account here. Nevertheless, this model seems to capture the essential elements of the overall local (atomic) and mesoscale order. In constructing this model for the framework of *h*-C_{18}PyReSeBr, we used bridging and bonding modes for the triselenide ligands and $[Re_6Se_8]$ clusters similar to those found in the crystallographically characterized $Cs_6Re_6Se_{15}$.[34] The latter is a 3D framework of octahedral $[Re_6Se_8]$ clusters linked with diselenide ligands according to the perovskite ReO_3 topology. An example where polyselenide units are known as ditopic strutlike ligands bridging metal atoms in a metal inorganic framework is found in $(Ph_4P)In(Se_6)_2$.[35] The bridging mode of the $[Se_3]^{2-}$ linkers in *h*-C_{18}PyReSeBr is similar to that observed for the $[Se_6]^{2-}$ linkers in the framework of $[In(Se_6)_2]^{1-}$.[35]

The pore structure and inorganic framework surface area of *h*-C_{18}PyReSeBr were characterized with small-angle X-ray scattering (SAXS) analysis. The SAXS technique can probe fluctuations in the electron density of matter on the nanoscale.[36] In mesostructured materials, which consist of regular arrays of pore channels embedded in an inorganic network, SAXS occurs primarily at the interface between the inorganic framework and

(34) Bronger, W.; Koppe, C.; Schmitz, D. *Z. Anorg. Allg. Chem.* **1997**, *623*, 242.
(35) Dhingra, S.; Kanatzidis, M. G. *Science* **1992**, *258*, 1769.
(36) Glatter, O.; Kratky, O. *Small-Angle X-ray Scattering*, Academic Press, New York, 1981.

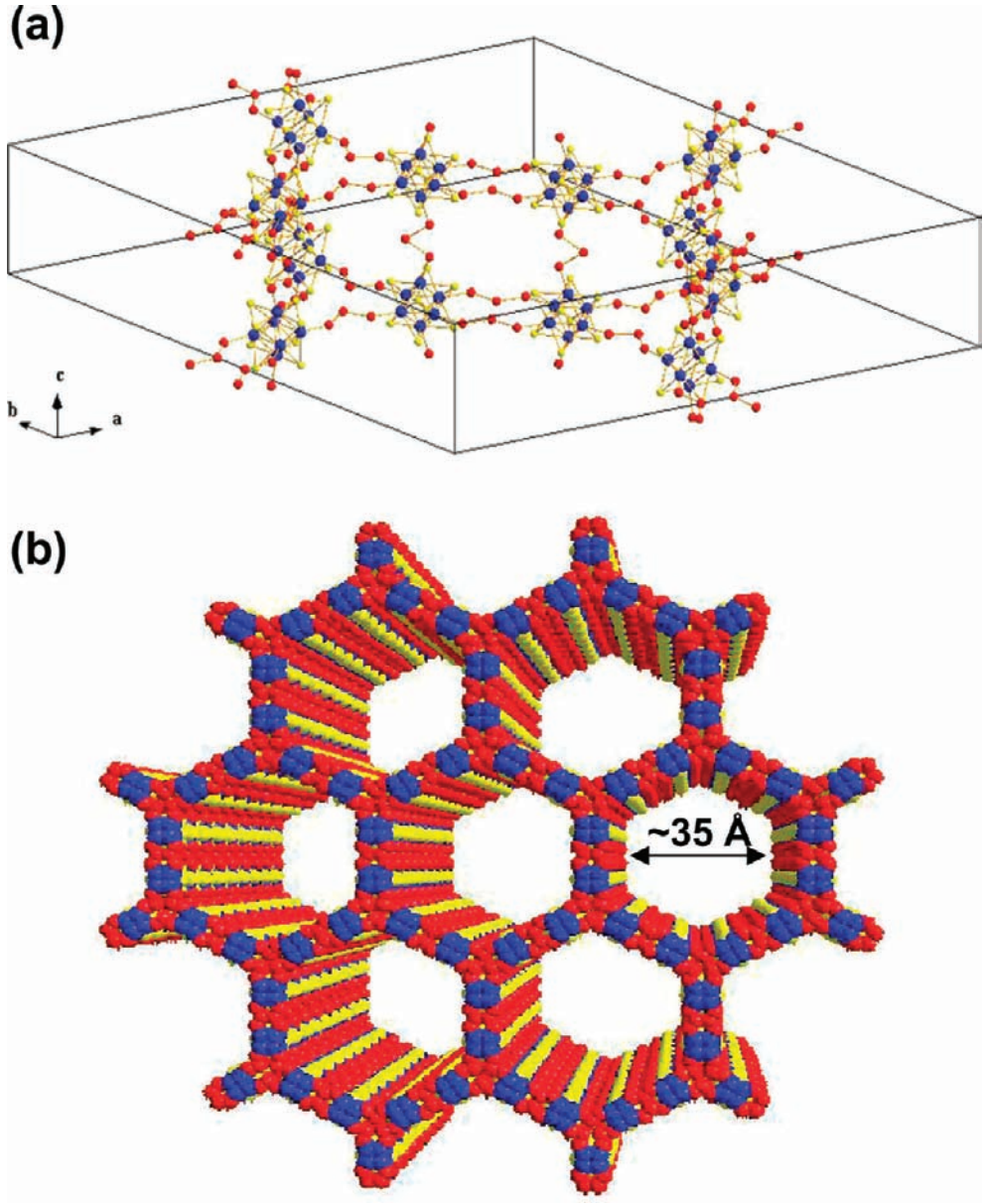

Figure 5. Structural model of *h*-C_{18}PyReSeBr with the composition of $(C_{18}Py)_{3.2}(Re_6Se_{7.2}Br_{0.8})(Se_3)_3$: (a) one unit cell and (b) a perspective view of the hexagonal inorganic framework. Organic surfactant molecules are not included in the structure. Blue atoms are Re, yellow atoms are mixed occupied Se/Br (designated as E in the text), and red atoms are Se.

the pore. It is irrelevant whether the pore is empty or filled as long as there is an electron density difference between the pore and the wall. Therefore, the SAXS technique can survey the total surface area of both open and surfactant-stuffed pores in a sample with good accuracy.[37] The SAXS-derived surface area was determined using the two-phase media approach.[36,37] The SAXS analysis performed on *h*-C_{18}PyReSeBr (Figure S2) indicated an interfacial area of ~477 m^2/g and a pore size of ~32 Å, which are very close to those determined from the structural model (interfacial area ~495 m^2/g and pore size ~35 Å). This is an enormous area between the inorganic framework and the guest surfactant cations, given the heavy elements that make up the framework, and when adjusted for density, it corresponds to an equivalent surface area of 738 m^2/g silica and 3648 m^2/g COF-108.[38]

It is noteworthy that *h*-C_{18}PyReSeBr is stable in air and even in acid. The acid treatment provides an opportunity for the removal of the surfactant cations by proton-exchange reactions. Figure 6a shows the powder XRD pattern of the materials before (*h*-C_{18}PyReSeBr) and after (*h*-H^+/C_{18}PyReSeBr) an H^+-exchange reaction. It is clear that the framework responds dynamically to this externally stimulated process and contracts along the *a* and *b* axes but retains its integrity (based on PDF analysis, see Figure 4c) and hexagonal pore symmetry. The Bragg reflections in the region of $2\theta < 6°$ of the H^+-exchange material indicate that the hexagonal pore arrangement is

(37) Armatas, G. S.; Kanatzidis, M. G. *Adv. Mater.* **2008**, *20*, 546.

(38) Equivalent surface areas are based on bulk density calculations and, assuming a mass bulk density of *h*-C_{18}PyReSeBr, MCM-41 silicate and COF-108 solids equal to 1.30 (Supporting Information), 0.84 (Edler, K. J.; Reynolds, P. A.; White, J. W.; Cookson, D. *J. Chem. Soc., Faraday Trans.* **1997**, *93*, 199), and 0.17(El-Kaderi, H. M.; Hunt, J. R.; Mendoza-Cortés, J. L.; Côté, A. P.; Taylor, R. E.; O'Keeffe, M.; Yaghi, O. M. *Science* **2007**, *316*, 268)g/cm^3, respectively.

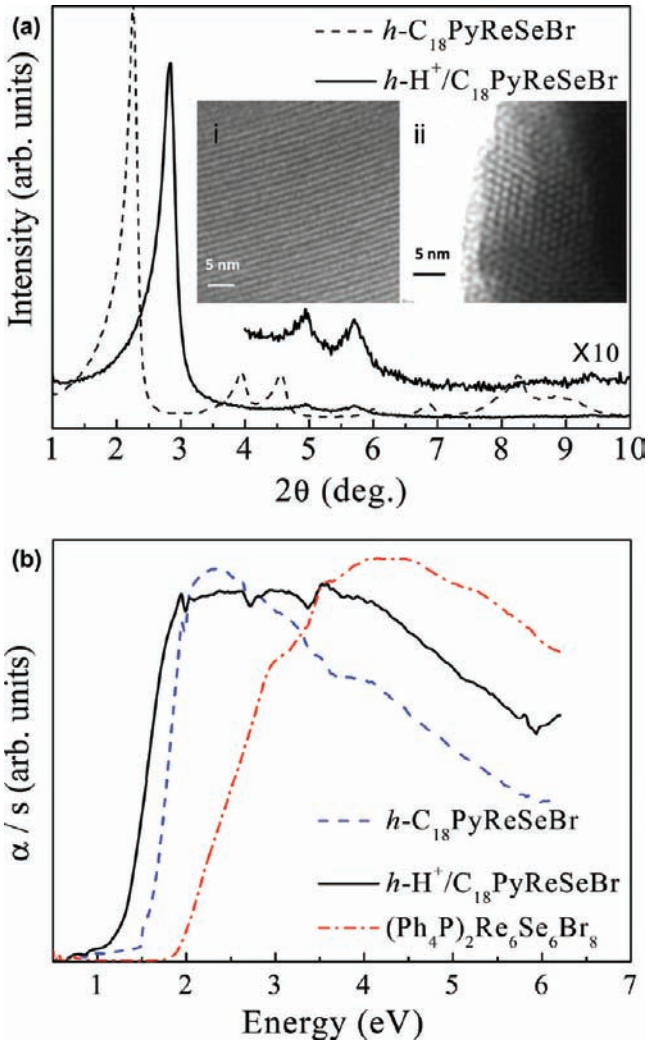

Figure 6. (a) Powder XRD patterns of pristine (---) and H^+-exchanged (−) *h*-C_{18}PyReSeBr materials. The insets show typical TEM images of *h*-H^+/C_{18}PyReSeBr taken (i) perpendicular to the pore channel axis and (ii) along the pore channel axis. (b) UV−vis absorption spectra of *h*-C_{18}PyReSeBr (---) and *h*-H^+/C_{18}PyReSeBr (−) and of the starting $(Ph_4P)_2Re_6Se_6Br_8$ (-·-) compound for comparison.

preserved after acid treatment. Typical TEM images of *h*-H^+/C_{18}PyReSeBr (Figure 6a, insets) clearly show a well-ordered hexagonal mesoporous structure. In comparison with the parent *h*-C_{18}PyReSeBr, the cell parameter of *h*-H^+/C_{18}PyReSeBr contracted from 44.5 to 35.8 Å, implying at least a 35% decrease in the unit cell volume, assuming that the *c* axis remains unchanged. Correspondingly, the thermogravimetric analyses showed ∼14.0% weight loss from 215 to 295 °C for the H^+-exchanged product whereas that of the parent material is ∼33.3% from 177 to 305 °C (Figure S3). Given that the ion-exchange reaction does not alter the framework composition and architecture, the proton-exchange yield was found to be ∼59%.

Both *h*-C_{18}PyReSeBr and *h*-H^+/C_{18}PyReSeBr are narrower band gap semiconductors compared to the starting cluster $(Ph_4P)_2[(Re_6Se_6Br_2)Br_6^T]$, with energy gaps at 1.56, 1.22, and 2.00 eV, respectively (Figure 6b). This suggests that the band gap transition of the $[(Re_6Se_6Br_2)Br_6^T]^{2-}$ cluster is red shifted upon coordination with the triselenide units.

Table 1. Elemental Analyses and Estimated Formulae of Pristine *h*-C_{18}PyReSeBr and the H^+-Exchanged Products

sample	C, H, and N[a]	EDS Re/Se/Br	estimated formula
h-C_{18}PyReSeBr	25.02, 3.59, 1.21 (25.07, 3.82, 1.27)	1:2.98:0.19	$(C_{18}Py)_{3.2}(Re_6Se_{7.2}Br_{0.8})(Se_3)_3$
H^+/C_{18}PyReSeBr	12.22, 1.80, 0.59 (12.40, 1.95, 0.63)	1:3.12:0.27	$H_{1.9}(C_{18}Py)_{1.3}(Re_6Se_{7.2}Br_{0.8})(Se_3)_3$

[a] The calculated C, H, and N fractions based on the formula from the structure model are given in parentheses.

On the basis of the structural model and the composition of *h*-C_{18}PyReSeBr given by elemental analysis, it appears that some Br atoms in the cluster core were replaced by Se^{2-} during the metathesis reaction. The replacement of a bridging halide atom that is part of the cluster core by external chalcogenide anions to produce a $[Re_6Se_8]$ core is a well-known reaction.[39] The composition of *h*-C_{18}PyReSeBr is $(C_{18}Py)_{3.2}(Re_6Se_{7.2}Br_{0.8})(Se_3)_3$, giving C, H, and N % equal to 25.07, 3.82, and 1.27, respectively, which agree very well with the experimental data (Table 1). ICP-AES(OES) elemental analysis experiments gave an Re/Se/Br atomic ratio of 3:8.2:0.36, which is in agreement with the proposed formula.

Concluding Remarks

We have obtained the unique, high-surface-area hexagonal metal inorganic framework *h*-C_{18}PyReSeBr by linking ditopic $[Se_3]^{2-}$ strutlike ligands with the octahedral cluster $[(Re_6Se_6Br_2)Br_6^T]^{2-}$. The samples are highly diffracting relative to surfactant-templated mesostructured materials but poorly diffracting relative to MOF crystals. We deduced a plausible suitable structural model that fits a broad set of experimental data. To our knowledge, this represents the first example of a mesoporous metal chalcogenide with a crystalline-like pore framework structure. To date, detailed structures of all surfactant-templated mesostructured materials are unknown because of the amorphous nature of the framework walls. The results presented here are a step closer to understanding such structural details, and this is possible because of the use of well-defined invariant building units (i.e., Re_6Q_8 clusters) that promote a more ordered framework. Because the Chevrel-type clusters are combined with structurally flexible $[Se_3]^{2-}$ linkers, the *h*-C_{18}PyReSeBr framework behaves dynamically upon ion exchange with protons and undergoes a huge (∼35%) volume change in the process. These results could serve as guide for the "design" of a wide variety of dynamically robust yet flexible metal inorganic frameworks.

Acknowledgment. This work was supported by the NSF. We thank P. Chupas (ANL) for help with the handling of the PDF data.

Supporting Information Available: Indexing of the powder XRD patterns, structural model details, and SAXS and TGA results. This material is available free of charge via the Internet at http://pubs.acs.org.

JA910506B

(39) (a) Yaghi, O. M.; Scott, M. J.; Holm, R. H. *Inorg. Chem.* **1992**, *31*, 4778. (b) Gabriel, J.-C. P.; Boubekeur, K.; Uriel, S.; Batail, P. *Chem. Rev.* **2001**, *101*, 2037.